Chapter 7
Life Prediction Under Multiaxial Complex Stress States of Variable Amplitude

7.1 Introduction

Every engineering structure sustains numerous different loading patterns during its daily operation. Loading patterns of constant amplitude represent the minority, while the majority of the applied loads are of an irregular nature. A characteristic of the realistic loading is the stress multiaxiality, since, even when the external loads are of a uniaxial nature, the developed stress and strain fields are normally more complicated due to the material anisotropy.

The understanding and modeling of the material behavior under fatigue loading and the prediction of the fatigue life are difficult tasks, which become more complicated when the loading is of variable amplitude. There are two different classes of approaches that address this task [1]. The first is based on the selection of a damage summation rule for the fatigue life prediction of the examined material, without any observation of the actual damage mechanisms that develop in the material and cause the failure. The most commonly used is the linear Miner's damage accumulation rule because of its simplicity and the limited requirement for fatigue data. However, as it has been reported, e.g., [2, 3], fatigue life predictions for GFRP and CFRP composite materials are not accurate when this rule is used. Therefore, other, non-linear, damage accumulation rules were developed and applied for different material systems and loading conditions, e.g., [4, 5]. The second approach is based on the selection of a damage metric, such as the residual strength, e.g., [6–8], or the stiffness of the material, e.g., [9–11]. These methods can model the variance of the selected damage metric during fatigue life and eventually predict the lifetime based on predetermined failure criteria.

These theories were developed mainly based on constant amplitude and block loading fatigue data. However, over the last three decades, more fatigue data have been produced in laboratories concerning fiber-reinforced composite materials in order to examine their behavior under realistic loading situations, including variable amplitude fatigue loading and complex environmental conditions,

A. P. Vassilopoulos and T. Keller, *Fatigue of Fiber-reinforced Composites*,
Engineering Materials and Processes, DOI: 10.1007/978-1-84996-181-3_7,

e.g., [12–18]. In parallel to the experimental work that is performed, theoretical models are developed for the simulation of the fatigue behavior of the examined materials under different thermomechanical loading conditions and the prediction of material fatigue life under complex stress states that may arise during the operation of a structure in the open air.

A fatigue life prediction methodology is usually based on the development of empirical relationships between the applied loads and the fatigue lifetime of the examined materials. The implementation of a numerical procedure for fatigue analysis consists of a number of distinct calculation modules, related to life prediction. Some of these are purely conjectural or of a semi-empirical nature, e.g., the failure criteria, while others rely heavily on experimental data, e.g., S–N curves and constant life diagrams (CLDs). In cases of composite laminates under uniaxial loading, leading to uniform axial stress fields, the situation can be substantially simplified since almost all relevant procedures could be implemented by experiment. On the other hand, for complex stress states, the laminated material is considered as being a homogeneous orthotropic medium and its experimental characterization, i.e., static and fatigue strength, is performed for both material principal directions and in-plane shear [19]. This *laminate approach* is a straightforward one for predicting fatigue strength under plane stress conditions, avoiding the consideration of damage modeling and interaction effects between the plies and stress redistribution, and can be reliably used when limited stacking sequence variations are present in a structural element. The approach was implemented by Philippidis and Vassilopoulos [17, 20–22] for a glass/polyester multidirectional laminate of [0/±45] stacking sequence and was shown to yield satisfactory predictions for fatigue strength under complex stress conditions for both constant amplitude and variable amplitude loading. A straightforward algorithm must be followed comprising at steps dealing with the analysis of the load to determine the developed stress fields, the interpretation of the fatigue data of the examined laminates to derive the S–N curves and the corresponding constant life diagrams, the fatigue failure criteria of the calculation of the design allowables and finally the damage accumulation based on the selected damage rule.

In large composite structures, consisting of numerous different materials and laminate configurations, a *lamina-to-laminate* approach seems more appropriate, although requiring the development of additional calculation modules that are able to take into account the implications in local stress fields, stress redistribution in neighboring plies and finally, how damage propagates as a function of loading cycles, e.g., [19, 23, 24]. In cases like this, the material properties of the basic building ply need to be experimentally derived. The properties of any new laminate configuration are then estimated based on existing theoretical procedures. The failure analysis is based on a progressive damage modeling, considering failed layers and stress redistributions in the laminate according to the applied load history.

It is obvious that whatever method will be followed for the life estimation, implementation of the necessary steps into a computer program is indispensable. Software products have been developed to assist the research community and simplify design processes. The methods implemented in the software packages

were based either on the micromechanics modeling of fatigue life, e.g. Helius:Fatigue [25] or the phenomenological laminate approach described above, e.g. *CCfatigue* [26].

In this chapter, a classic fatigue life prediction methodology (based on the laminate approach) is presented and applied to the constant and variable amplitude fatigue experimental data from Chap. 2 in order to examine the accuracy of the predictions. The effect of the various parameters of the proposed methodology on the final life prediction result is investigated. The application of the methodology is assisted by the recently developed computational tool *CCfatigue* [26]. *CCfatigue* is a modular software framework that allows rapid interchange between modules in a complete fatigue life prediction methodology and the evaluation of their effect on the life prediction results. A software library has already been developed, containing a significant number of solutions for each step of the fatigue life prediction methodology.

7.2 Classic Fatigue Life Prediction Methodology

The estimation of fatigue life based on classic fatigue life prediction methodology comprises at a number of sequentially executed modules. Therefore, a classic life prediction methodology can be considered as an articulated method consisting of four to five basic steps:

- Cycle counting, to convert variable amplitude (VA) time series into blocks of certain numbers of cycles corresponding to constant amplitude and mean values.
- Interpretation of fatigue data to determine and apply the appropriate S–N formulation for the examined material.
- Selection of the appropriate formulation to take the mean stress effect on the fatigue life of the examined material into account.
- Use of the appropriate fatigue failure criterion to calculate the allowable number of cycles for each loading block that results after cycle counting.
- Calculate the sum of the partial damage caused to the material by each of the applied loading blocks estimated using the cycle-counting method.

Modeling constant amplitude fatigue behavior involves the determination of the S–N curves (plot of cyclic stress vs. life), typically by grouping data at a single R-value ($\sigma_{\min}/\sigma_{\max}$) (incidentally, depending on the R-value, an S–N curve can be constructed from data obtained at varying mean and amplitude). Interpretation of the fatigue behavior for the assessment of the mean stress effect results in the construction of the constant life diagram (CLD). These two processes can be treated as separate steps, but are related in the sense that the CLD is constructed from the available S–N curves, and new S–N curves could be extracted from this CLD.

The flowchart presented in Fig. 7.1 shows the procedure followed in order to calculate the damage index for a given variable amplitude fatigue problem. Information regarding the 2nd, 3rd and 4th steps that concern the interpretation of

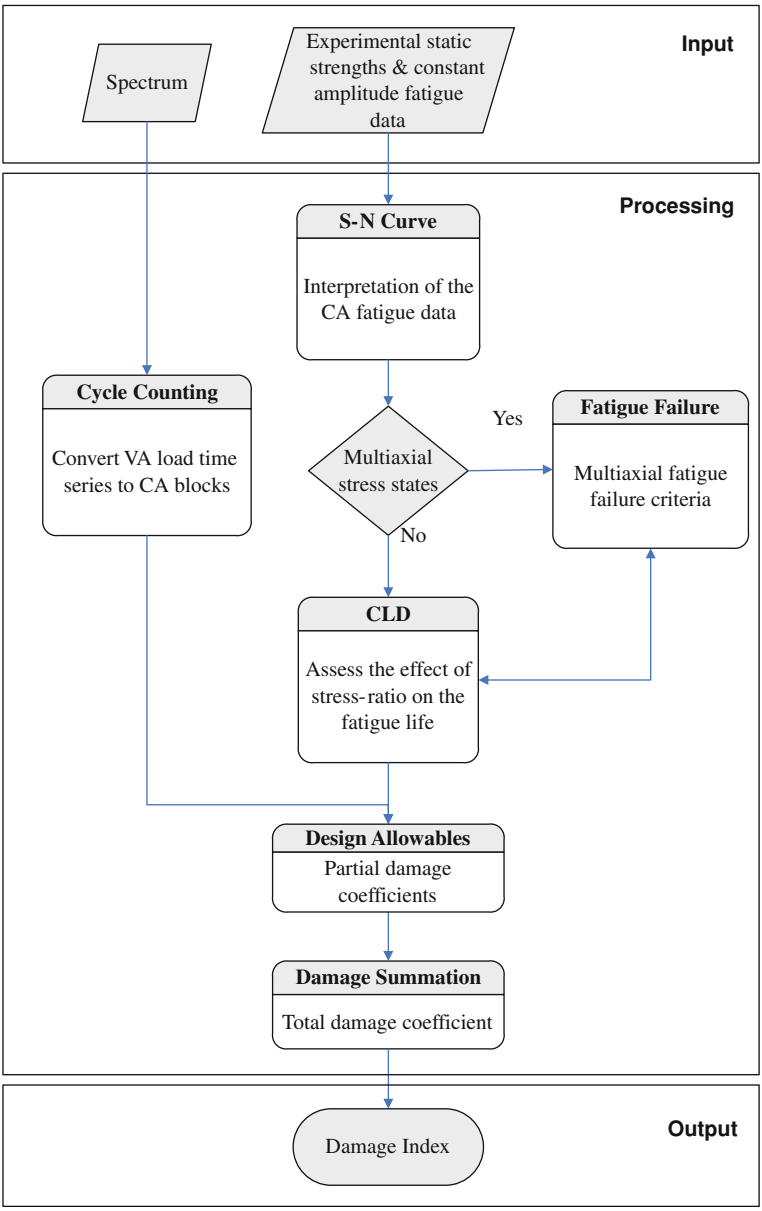

Fig. 7.1 Classic fatigue life prediction methodology flowchart

the fatigue data (Chaps. 3 and 4), constant life diagrams (Chap. 4) and fatigue failure criteria (Chap. 5) can be found earlier in this volume. The cycle-counting methods and damage accumulation rules will be briefly described here.

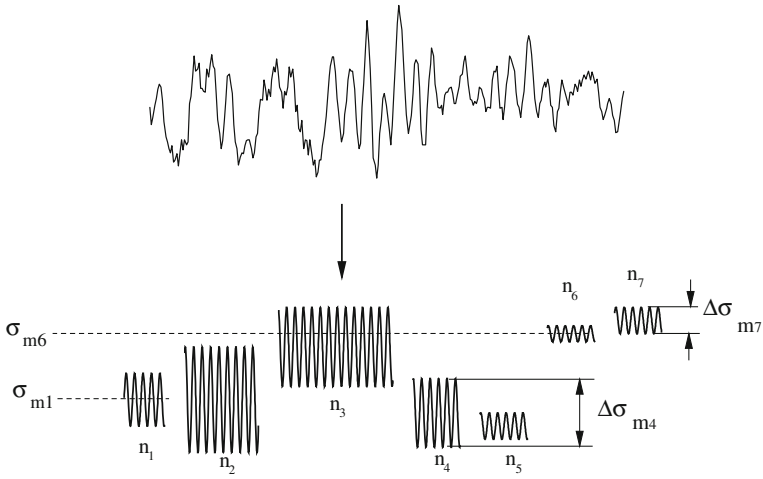

Fig. 7.2 Schematic representation of application of a cycle counting method

7.2.1 Cycle Counting

Cycle counting is used to summarize (often lengthy) irregular load vs. time histories by providing the number of occurrences of cycles of various sizes, see Fig. 7.2. The definition of a cycle varies with the method of cycle counting. A significant number of cycle-counting techniques have been proposed over the last 30 years, e.g., [27]. Typical events observed in a load-time history are the occurrence of load peaks or valleys at specific levels, the exceeding or "crossing" of specific levels and the occurrence of load changes or "ranges" of a specific size. Accordingly, cycle-counting methods can be classified as follows:

- Level-crossing counting methods.
- Peak counting methods.
- Simple range-counting methods and
- Rainflow counting methods.

Level-crossing, peak counting and simple range counting are designated one-parameter methods since they result in the counting of solely one load parameter. On the other hand, range-mean and rainflow-related methods are designated two-parameter methods and are more appropriate for the fatigue analysis of composite materials since they count how many times a cycle of specific range and mean value occur in a spectrum, thus taking into account the effect of mean stress on the fatigue life of the examined material.

The application of a cycle-counting method and storage of its results require a preliminary treatment of the loading, which consists of sampling, extraction of maximum and minimum loads and finally quantification of the values into classes.

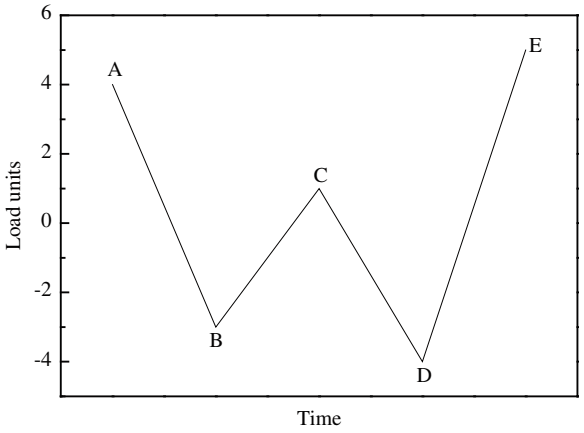

Fig. 7.3 Schematic representation of single-range counting principle

Sequences are generally produced by the monitoring of a continuous variable over time. Signal processing is then used to convert analog signals into digital ones, which consist of discrete digital values. Sampling is necessary because the digital signal has to correctly represent the evolution of the variable. Sequences of force, stress, strain or other loading parameters can be stored. These sequences are known as load-time histories.

Cycle-counting methods consider only the successive extremes of a load-time history and the sampled sequence is therefore reduced to a peak/valley sequence before cycle counting. Depending on which method is used, peaks or valleys or both may be required. In the classification of peaks and valleys a specific "range filter" is usually applied to remove low-range cycles from the sequence. The reversal points remaining after the search for peaks and valleys are discarded. Cycle-counting algorithms are then applied to the reduced load-time history, which count ranges as cycles using counting principles.

Two main principles can be applied for the cycle counting: the single-range or range-mean counting and the range-pair counting principle, on which rainflow counting is based as well. According to the single-range counting, Fig. 7.3, any transition from a peak, e.g. A, to a valley e.g. B, in a time series or from a valley B to a peak C, forms one half cycle with range = |A–B| and mean = (A + B)/2, or range = |B–C| and mean = (B + C)/2. Counting in single ranges results in as many half cycles as the number of load transitions in the loading sequence.

The rainflow counting and the earlier range-pair methods are used to extract hysteresis loops from a load history. The algorithm of counting cycles, based on the comparison of four successive data points of the loading history, is schematically shown in Fig. 7.4. The concept of stress–strain hysteresis loops resulting from a certain load history is visualized in Fig. 7.5.

A comprehensive description of the available cycle-counting methods for the analysis of spectra applied to composite materials is given in [28]. As mentioned in [28] the history of cycle-counting methods goes back to the 1950s and 1960s when

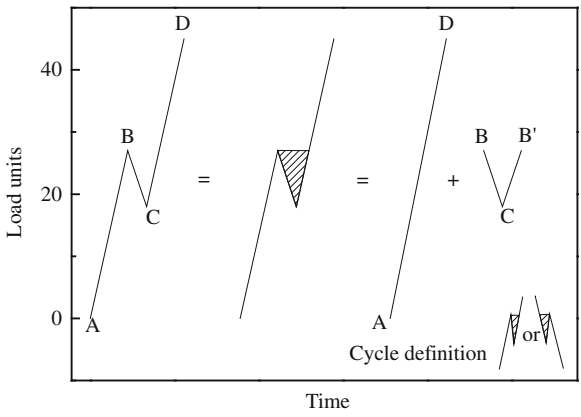

Fig. 7.4 Schematic representation of range-pair counting principle

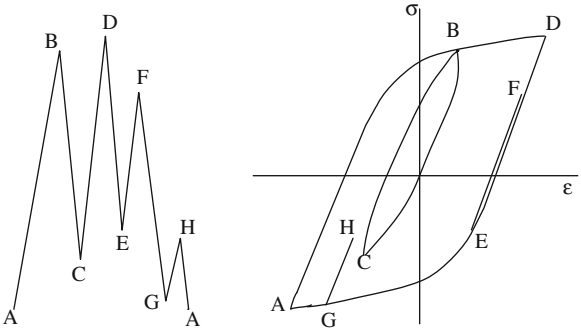

Fig. 7.5 Stress–strain hysteresis loops resulting from rainflow counting of an irregular spectrum

only simple range-counting or range-mean counting methods were used. The drawback of these methods is their inability to take into account the stress–strain history to which the material is subjected, and consequently their tendency to miss the largest overall load cycle in a sequence. The rainflow counting and related methods were introduced to address this problem [29–31]. Based on these algorithms, stress–strain hysteresis loops are counted rather than stress range and mean values. Endo et al. [29, 30] in Japan developed an algorithm that became known as the rainflow or "pagoda-roof" counting method. At the same time, in Europe, a two-dimensional method was developed by de Jonge [31] designated the "range-pair-range" or just "range-pair" method. Although based on different backgrounds, both cycle-counting algorithms yielded the same results when counting an arbitrary loading sequence.

Rainflow-counting, range-pair and range-mean methods seem the most appropriate for the analysis of composite material fatigue data, giving similar cycle-counting results for most practical applications [32]. However they present a number of deficiencies: rainflow-counting cannot be used for cycle-by-cycle analysis and it is therefore difficult to apply this method in combination with a residual strength fatigue theory. On the other hand, range-pair and range-mean

counting mask the presence of large and damaging cycles. Based on the previous comments, it is concluded that—according to the application and material used–the appropriate cycle-counting technique should be selected very carefully.

In this work, rainflow-counting, range-mean and range-pair counting methods are implemented in the fatigue life prediction methodology. The influence of the selection of the cyclic counting method is assessed by the predictive ability of the entire methodology.

7.2.2 Damage Accumulation

The last module in the life prediction algorithm is the accumulation of damage, which is carried out according to the linear Palmgren-Miner or the Miner rule. The number of operating cycles, n, of each bin, derived from rainflow counting, is divided by the allowable number of cycles, N_f (derived directly using the S–N curve equation, when a uniaxial fatigue stress state develops or by the solution of the fatigue failure criterion for N_f, when multiaxial fatigue stress fields are present) to form a partial damage coefficient. The summation of all partial damage coefficients and comparison with unity indicate whether the material will survive the application of the VA loading under consideration.

Various non-linear damage accumulation models have been proposed as alternatives to the Miner rule to improve the life prediction for anisotropic composites under VA loading. However, these "rules", mainly developed for two-stage and/or multi-stage block loading tests, cannot be applied for spectrum loading, especially in the case of anisotropic composites.

The difference between the Miner and non-linear damage summation rules is schematically presented in Fig. 7.6. For the linear damage rule, the damage caused to the material is the same for the same number of applied cycles and there is no relation to the history, i.e., the amount of existing damage to the material. On the other hand, when a non-linear rule is selected (simple cases are used for the example in Fig. 7.6) the damage accumulation is not linear, depending on rule type.

Non-linear "rules" yield more accurate life predictions than the Miner rule, simply because they are fitted to VA experimental data. They cannot be used for design purposes where numerous different load cases, composed of different spectra, must be examined. In this respect, they are not really damage accumulation rules.

An extensive review of existing cumulative damage models, not only for metals but also for composite materials, can be found in [33]. One of the simpler non-linear rules was introduced by Marco and Starkey [2] and assumes that damage accumulation is a function of the cyclic stress level:

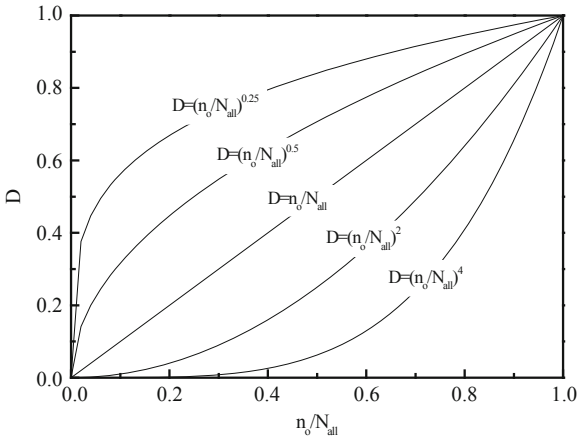

Fig. 7.6 Schematic representation of linear and non-linear damage accumulation rules

$$D = \sum_{i=1}^{k} \left[\left(\frac{n_{oi}}{N_{fi}} \right)^{a_i} \right] \tag{7.1}$$

where the parameter a_i is a function of stress level and must be estimated based on available experimental data.

Owen and Howe [5] developed a stress-independent non-linear cumulative damage model for chopped strand mat GRP, given by:

$$D = \sum_{i=1}^{k} \left[A \left(\frac{n_{oi}}{N_{fi}} \right) + B \left(\frac{n_{oi}}{N_{fi}} \right)^2 \right] \tag{7.2}$$

A modification of this model with the quadratic exponent replaced by another variable parameter was presented in [3]:

$$D = \sum_{i=1}^{k} \left[A \left(\frac{n_{oi}}{N_{fi}} \right) + B \left(\frac{n_{oi}}{N_{fi}} \right)^c \right] \tag{7.3}$$

In the above equations, n_{oi} and N_{fi} are the numbers of operating cycles and cycles to failure, respectively of the *i*th bin. In [2], the three parameters, A, B and c, were calculated using an iterative procedure to fit Eq. 7.3 to the experimental data. The same model, Eq. 7.3, was also used for the life prediction of CFRP angle-ply and pseudo-isotropic laminates tested under the FALSTAFF (Fighter Aircraft Loading STAndard For Fatigue) spectrum [34] and to predict the variable amplitude fatigue behavior of glass-fiber reinforced polyester laminates used for the construction of wind turbine rotor blades [17].

7.3 Life Prediction

The above described classic fatigue life prediction methodology is used in the following in order to estimate the lifetime of the examined material. Constant amplitude fatigue and static strength data from Chap. 2 were used for the implementation of the algorithm. Whenever available, static strength values used for the determination of CLDs were those derived from static tests at strain rates similar to those realized during the VA tests. Fatigue data were processed statistically and S–N curves at any reliability level could be estimated. However, in this chapter, curves corresponding to a 50% reliability level were used to produce life prediction results that can be compared with the experimental variable amplitude fatigue data also presented in Chap. 2.

7.3.1 Configuration of the Classic Life Prediction Methodology: Presentation of CCfatigue Software

Several modules were developed for the solution of each of the successive steps of the previously described classic fatigue life prediction methodology. Four cycle-counting techniques were implemented in the library of the *CCfatigue* software, four S–N curve formulations, five different methods for the construction of constant life diagrams, six multiaxial fatigue failure criteria for the calculation of the allowable number of cycles under the developed stress states and two methods for the damage accumulation: the linear Miner's rule and the non-linear equation described in the previous sections, Eq. 7.3, for the summation of the accumulated damage and assessment of the lifetime of the examined material. The *CCfatigue* framework is thus capable of predicting the fatigue life of a number of different material systems under different loading conditions. The flowchart of the methodology is presented in Fig. 7.1, which schematically shows the process used for predicting the Miner's damage index for a variable amplitude fatigue problem. The five distinctive steps of the methodology are presented in this section showing the data processing part of the software framework. The current version of *CCfatigue* offers 1,344 solver combinations, showing its capacity to address a wide range of materials and loading combinations.

The software framework and the existing modules are briefly introduced in this paragraph. The home page is shown in Fig. 7.7 and the five successive steps can be seen on the left hand side of the above screen shot. The user can run each step independently of the others, select the desired solver from those available in the software library and obtain the solution. The data structure of the output file for each step has been designed in such a way that it can be used as the input file for the following step. The implementation of the software for the life prediction of the selected materials and evaluation of the selected modules for each step are presented in the following sections.

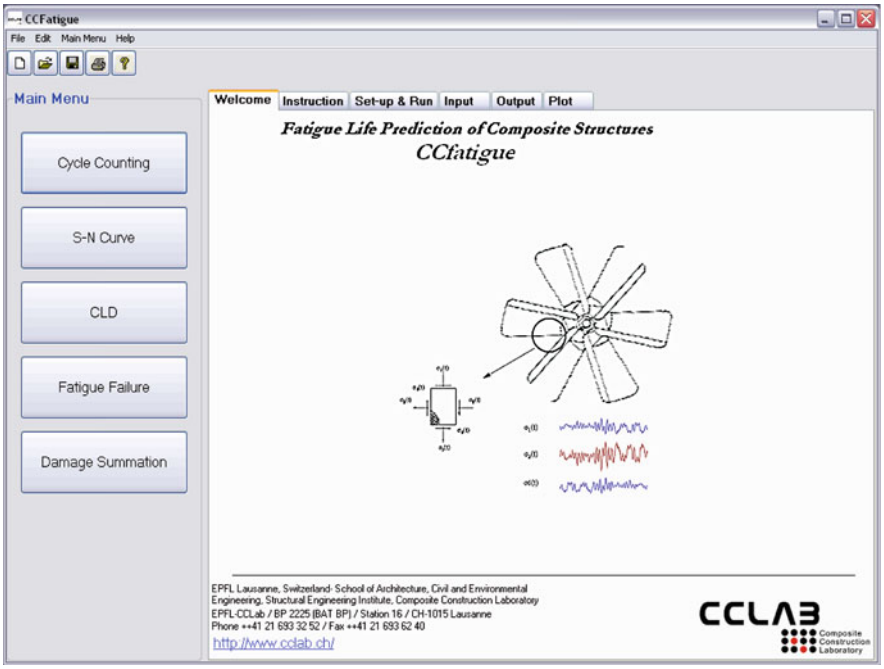

Fig. 7.7 *CCfatigue* software home page

A demonstration of the application of the software to solve each step of the methodology using different solvers and a brief discussion of their effect on the modeling of the exhibited fatigue behavior of the examined material under the given variable amplitude follows.

Cycle counting of both irregular spectra, presented in detail in Chap. 2, can be performed following the algorithms of the four methods implemented in the *CCfatigue* software. The cumulative spectra of the MWX and EPET573 spectra presented in Figs. 7.8 and 7.9, respectively show that there is no significant discrepancy if different methods are employed for counting the loading cycles. In general, all methods count the same or at least similar numbers of cycles, except range-mean which counts more cycles than the other three. In addition, the cumulative spectrum resulting from the application of the range-mean counting method is slightly different from the others, presenting more low-range cycles than the rainflow, simplified rainflow and range-pair counting algorithms.

The application of different S–N curve methods is demonstrated in Fig. 7.10 on fatigue data recorded after the application of compression fatigue loading ($R = 10$) to on-axis specimens. As shown, all S–N curves model the exhibited fatigue behavior similarly in the region between 10^3 and 10^6 cycles, but they are significantly different in the low- and high-cycle fatigue regimes. Depending on the cycle-counting results, each method can produce a conservative on

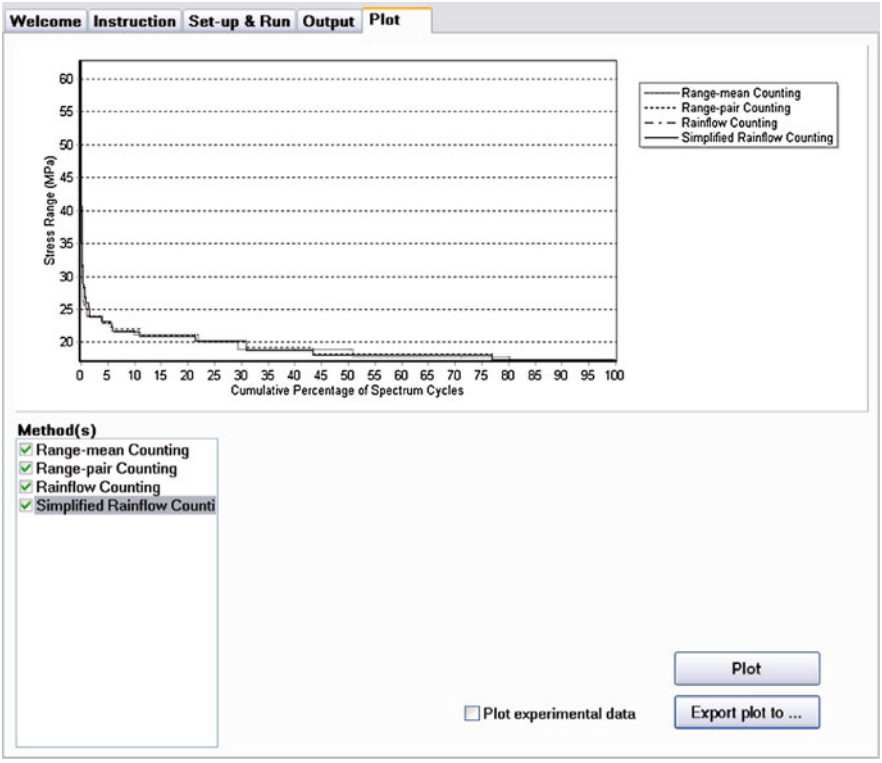

Fig. 7.8 Comparison of cumulative spectra resulting from different cycle-counting routines; MWX time series

non-conservative lifetime estimation. If the cumulative spectrum contains a significant percentage of high-range cycles for example, corresponding to low-cycle fatigue, use of Lin-Log or Log-Log relationships will yield conservative lifetime estimations, while use of the Sendeckyj method will yield non-conservative lifetime estimations.

The selection of the CLD also affects the final fatigue life prediction in a similar manner. As presented in Fig. 7.11, different CLD methods produce different diagrams and eventually estimate different S–N curves for desired stress ratios. Therefore, depending on the accuracy with which the CLD formulation estimates an S–N curve, fatigue life prediction can be accurate, conservative or non-conservative. The application of three methods—piecewise linear, Boerstra and piecewise non-linear (see Chap. 4 for explanations)—to the examined composite material system of Chap. 2 is demonstrated in Fig. 7.11. As shown, piecewise linear and non-linear diagrams are more conservative than Boerstra and therefore the use of one of these solutions would eventually yield more conservative fatigue life prediction results.

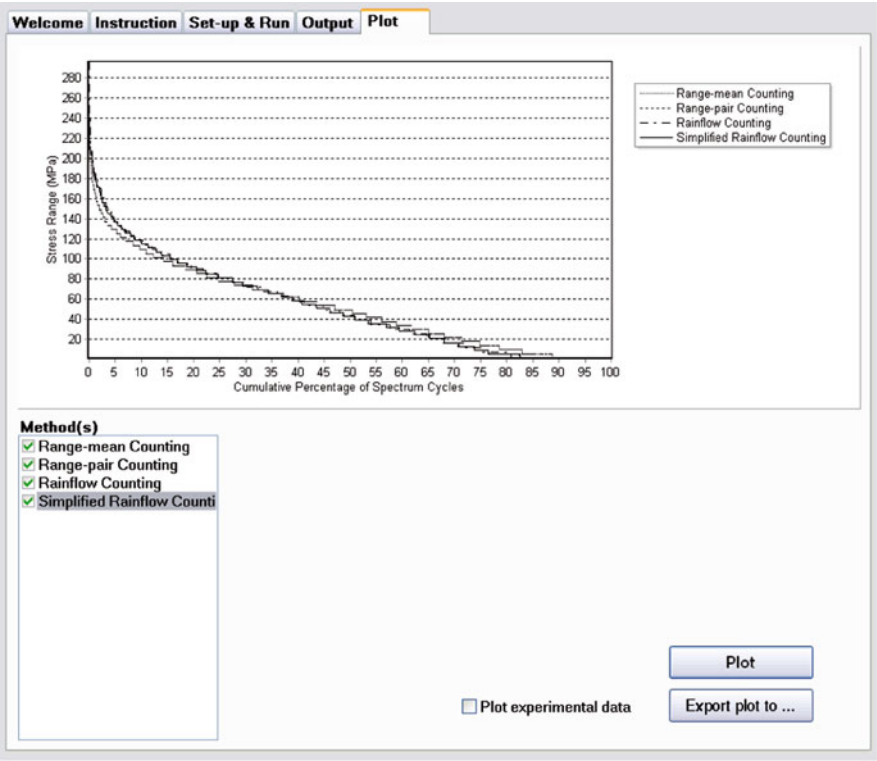

Fig. 7.9 Comparison of cumulative spectra resulting from different cycle-counting routines; EPET573 spectrum

In cases where a uniaxial stress state develops in the examined material, the next step, related to fatigue failure criterion selection can be omitted as selection of the appropriate S–N curve and CLD formulations suffices to take the effect of any possible variable amplitude loading pattern into account.

However, when the loading or resulting stress field is complex, constant life diagrams must be available for all strength parameters of the material in its symmetry directions, and the aforementioned interpolation procedure must be performed separately for all the plane stress tensor components. Their interaction in determining failure is then taken into account by considering multiaxial fatigue strength criteria. Six models were implemented in *CCfatigue* to cover as many concepts that deal with this problem as possible. Three of the selected models, Hashin-Rotem (HR), Sims-Brogdon (SB) and Failure Tensor Polynomial in Fatigue (FTPF)—see Chap. 6 for details—can be characterized as the macroscopic fatigue strength criteria, which are usually generalizations of known static failure theories for taking factors relevant to the fatigue life of the structure into account, such as number of cycles and loading frequency. Two more criteria, one proposed by Kawai (KW) and the second by Fawaz and Ellyin (FWE), seem very promising

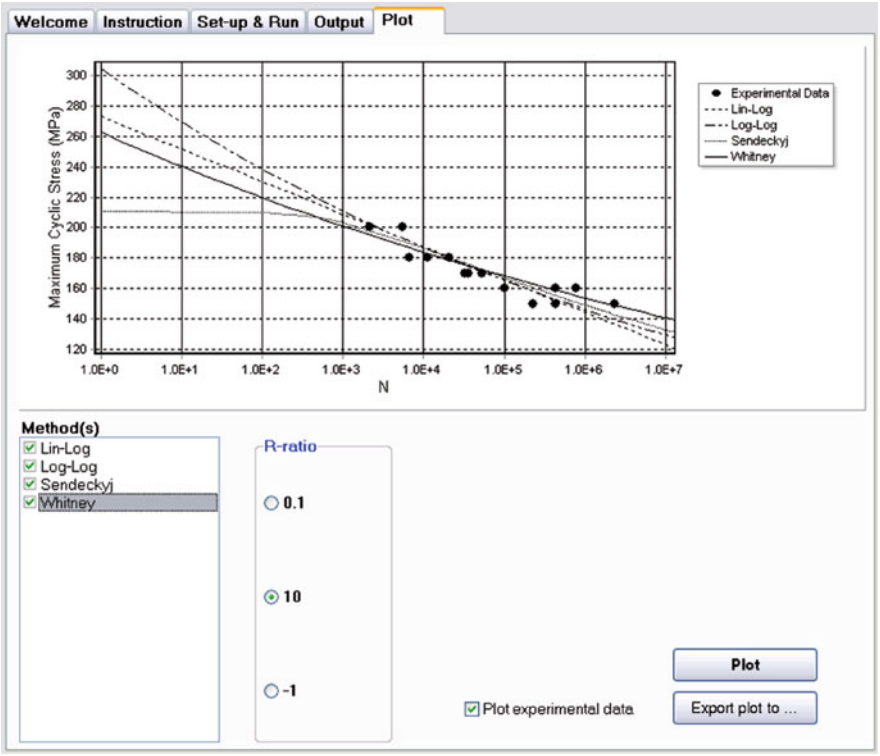

Fig. 7.10 Different types of S–N curves produced by *CCfatigue*

since they include the stress ratio in their formulation and can therefore be used without the need for any CLDs and are consequently based on limited databases. The sixth model, introduced by Shokrieh and Taheri (ST), is based on a strain energy concept and its use is also limited to the modeling of the off-axis fatigue behavior of unidirectional materials.

Although other models can be found in the literature, those selected here have been proved more accurate than others—see Chap. 6—and can be easily implemented in *CCfatigue* and fatigue databases that exist in the literature for the evaluation of their accuracy. The *CCfatigue* interface for selection of the appropriate fatigue failure theory and input of the requested parameters is presented in Fig. 7.12 (the HR criterion is used for the demonstration). The static-tensile and compressive strengths of the material are required as input together with three S–N curves (normally those corresponding to the fatigue functions of the material along the longitudinal and transverse directions and under shear). Use of the selected criterion allows the prediction of the S–N curve for the examined material system at any off-axis angle.

Damage summation is performed during the last step of the *CCfatigue* software framework—a typical "Set-up & Run" tab is presented in Fig. 7.13. The

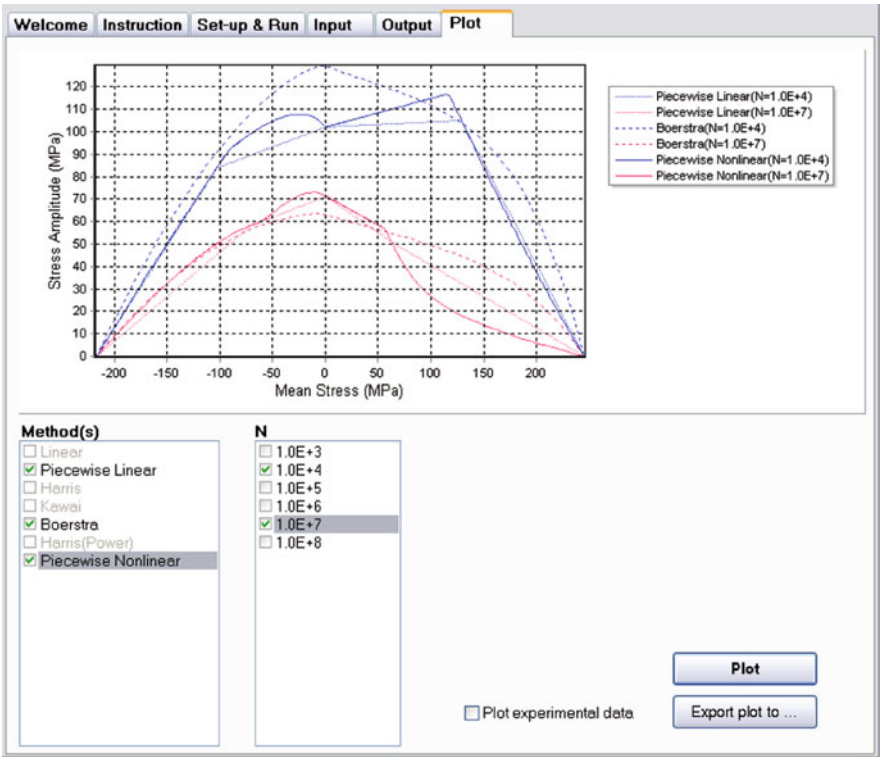

Fig. 7.11 Typical piecewise linear, Boerstra and piecewise non-linear diagrams for 10^4 and 10^7 cycles derived using *CCfatigue*

combination of the solvers for the solution of each step of the articulated methodology can be selected in the interface. A fatigue damage index is the output of this module, corresponding to the damage accumulated in the material after application of the selected fatigue spectrum. In the present version of the software, the linear Miner rule and the non-linear equation described earlier Eq. 7.3 were implemented.

7.3.2 Application of the Classic Fatigue Life Prediction Methodology

The classic fatigue life prediction methodology was applied to the fatigue data of the examined material in order to evaluate its predictive ability. The theoretical predictions were compared to variable amplitude experimental data under the modified version of the standardized WISPERX spectrum, designated MWX in Chap. 2, and an alternative variable amplitude spectrum, designated EPET573.

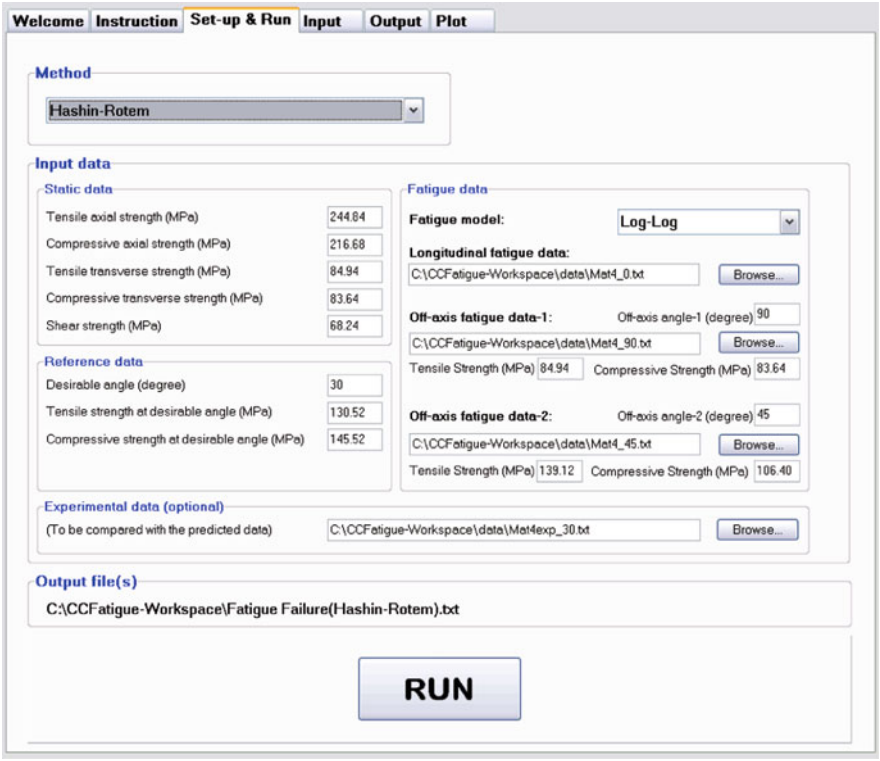

Fig. 7.12 *CCfatigue* interface for setting-up of fatigue failure solver

The following configuration of the *CCfatigue* software framework was selected with the chosen solvers being the most common for each step:

- Rainflow cycle-counting method,
- Log-Log S–N curve formulation,
- Piecewise linear constant life diagram,
- Miner's damage rule.

In cases where multiaxial stress states developed in the material, the Failure Tensor Polynomial in Fatigue (FTPF), described in Chap. 6, was employed to calculate the allowable number of cycles for the developed stress state.

A comparison of theoretical predictions with experimental data is presented in Figs. 7.14, 7.15, 7.16 and 7.17. Experimental data points from variable amplitude tests with MWX are compared with theoretical predictions, shown as solid lines, in Fig. 7.14 for on-axis and in Fig. 7.15 for off-axis tests. In general, the theoretical numbers of spectrum passes are found to be in satisfactory agreement with the experimental values. Nevertheless, this is not the case for specimens tested under the alternative spectrum EPET573, Figs. 7.16 and 7.17, for which conservative predictions resulted, especially those regarding the on-axis data. Therefore it can

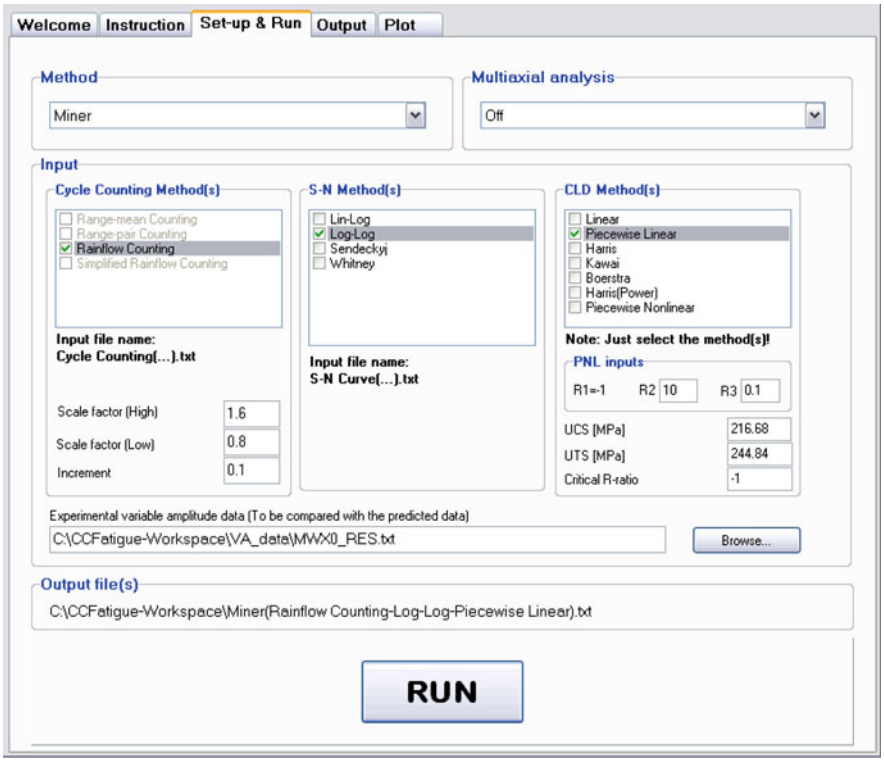

Fig. 7.13 Fatigue life prediction estimation based on selected modules

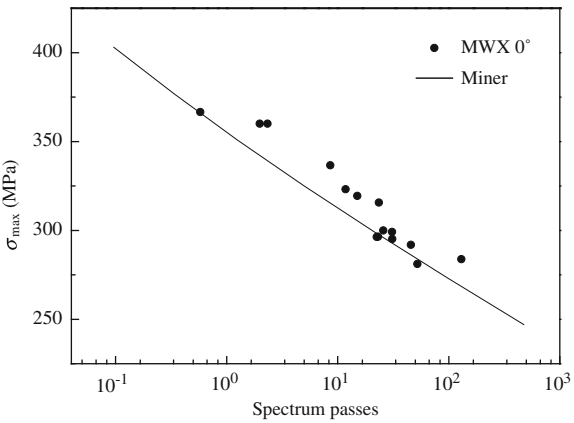

Fig. 7.14 Theoretical predictions vs. experimental data for 0° on-axis specimens; MWX spectrum

be concluded that the predicting efficiency of the methodology, in the present framework, is not affected by fiber lay-ups, but by the spectrum itself. For the more "irregular" EPET573 spectrum, results are less accurate, while for the MWX

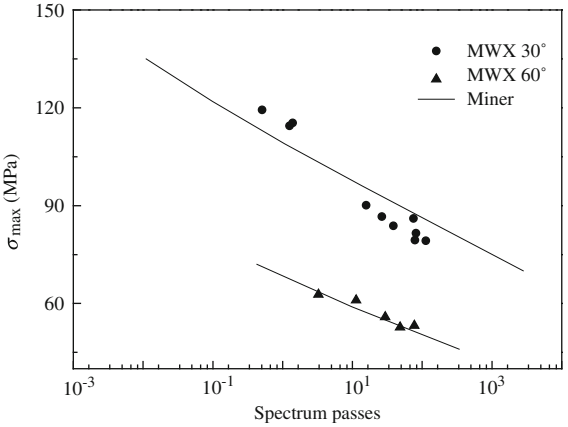

Fig. 7.15 Theoretical predictions vs. experimental data for 30° and 60° off-axis specimens; MWX spectrum

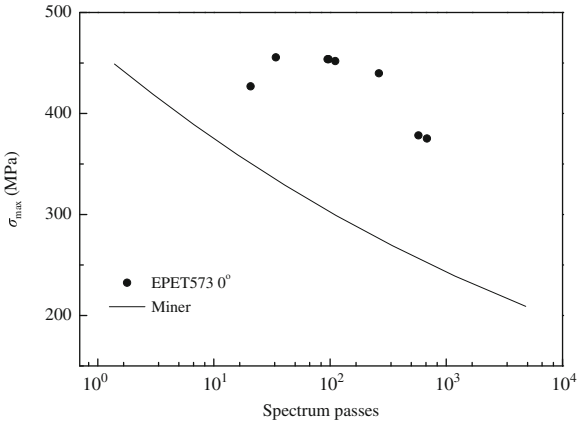

Fig. 7.16 Theoretical predictions vs. experimental data for 0° on-axis specimens; EPET573 spectrum

spectrum, which is almost a sequence of block loading patterns, relatively accurate predictions can be achieved irrespective of fiber orientation. Discrepancies observed between theory and experiment in the latter case could possibly be caused by any one of the algorithm modules described.

Since the fatigue failure criterion is not used for predicting the response of on-axis loaded specimens for which, as shown in Fig. 7.16, the greatest discrepancies are observed, it is concluded that either CLD resolution, implemented by interpolating between S–N curves at three *R*-ratios and static strengths, or the S–N curve formulation, or the Miner's damage accumulation rule could be the cause of the problem. Each of the above or their combination can drastically affect prediction accuracy. The S–N curves, for example, were used successfully for the life prediction of specimens subjected to the MWX spectrum, see Fig. 7.14, but their validity is questioned when the EPET573 spectrum is used, see Fig. 7.16. This could be explained by the fact that MWX is a sequence of blocks of constant

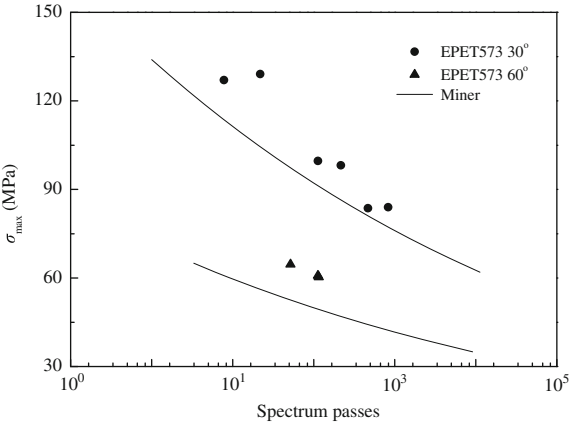

Fig. 7.17 Theoretical predictions vs. experimental data for 30° and 60° off-axis specimens; EPET573 spectrum

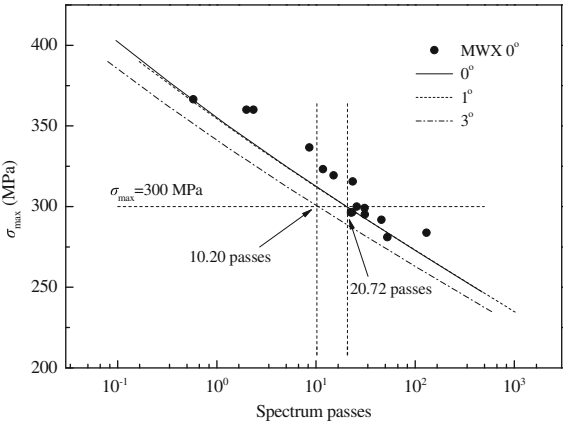

Fig. 7.18 Effect of load misalignment on life prediction of specimens cut at 0° on-axis; MWX spectrum

high-range cycles and that the present S–N formulation is found to be adequate. On the other hand, the EPET573 spectrum consists of many low-range cycles, see Fig. 7.20 in Chap. 2, and for these stress ranges the S–N curves must be extrapolated far beyond 10^7 cycles to determine the allowable number of cycles. However, the derived S–N curves are extracted from test data between approximately 10^3 and 3×10^6 loading cycles and are obviously not representative for the region beyond 10^7 cycles.

The damage accumulation rule and associated rainflow counting, which implies the use of Miner's rule, could also affect life prediction; by comparing the two variable amplitude time series (Figs. 2.17 and 2.18 in Chap. 2), and their cumulative spectra (Figs. 7.8 and 7.9) clearly show that the application of EPET573, consisting of alternating high- and low-range cycles, would result in pronounced load sequence effects.

Regardless of the effect of various parameters on the accuracy of the theoretical predictions, a strong effect of the plane stress state was observed in comparisons

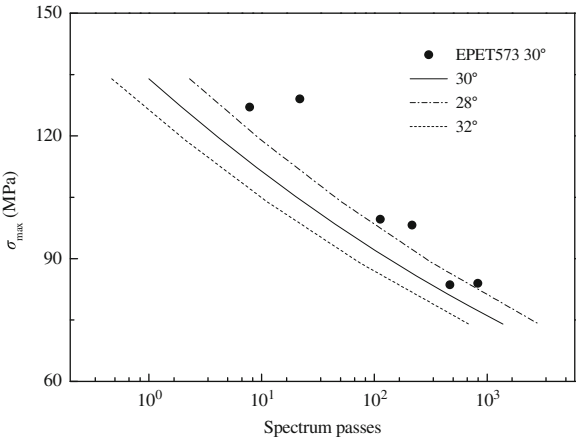

Fig. 7.19 Effect of load misalignment on life prediction of specimens cut at 30° off-axis; EPET573 spectrum

with data from both test series. For on- and off-axis loading, even a few degrees of misalignment yielded substantially different theoretical predictions as shown in Figs. 7.18, 7.19 for both MWX and EPET573 loading spectra. This proves the significant role of transverse-to-the-fiber normal and shear stress components in the failure of the laminate investigated, since even slight deviations of the loading direction affect σ_2 and σ_6 values in the principal material system and drastically change the expected number of passes of both load spectra. A misalignment of two degrees, for example, from the ideally axial loading direction, produces a plane stress state with $\sigma_1 = 99.9\%$ of σ_x, $\sigma_2 = 0.1\%$ of σ_x and $\sigma_6 = 0.035\%$ of σ_x. However, despite the low values of transverse normal and shear stress components, life prediction is apparently affected as shown for example in Fig. 7.18 for specimens cut at 0° and tested under the MWX spectrum and also in Fig. 7.19 where predictions for specimens cut at 30° and tested under EPET573 loading spectrum are shown.

Care should be also taken regarding the selection of the data used as baseline. Different damage coefficients would be calculated if Log-Log or Lin-Log curves are used for S–N data representation as mentioned in [16]. Moreover, even UTS or UCS values, used for determination of the constant life diagrams, could drastically affect the expected lifetime. As was mentioned earlier, for the construction of the CLDs, ultimate stress values derived at strain rates similar to those realized in the VA series were used, wherever available. These values were significantly greater than corresponding values determined in static tests, performed according to relevant standards, and indeed, as shown in Figs. 7.20, 7.21, they affect the expected life predictions for both loading spectra. As can be seen from Fig. 7.20, the use of the UTS derived at a high strain rate leads to the accurate prediction of the fatigue life of specimens cut at 0° and tested under the MWX spectrum, while use of a lower value of the UTS derived at a standard test speed yields conservative predictions. The difference in predictions also exists when the fatigue behavior of

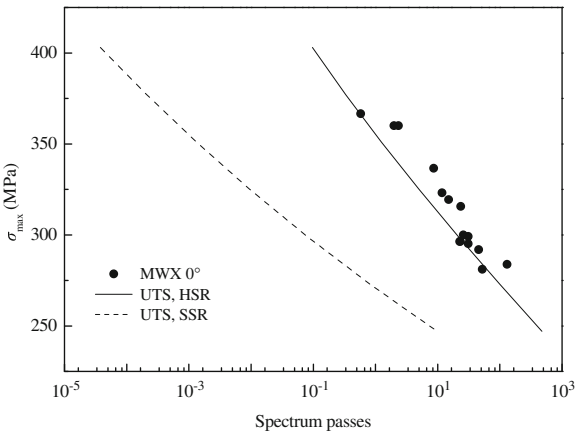

Fig. 7.20 Effect of ultimate tensile stress on life prediction results. MWX spectrum applied on-axis (HSR: high strain rate, SSR: standard strain rate)

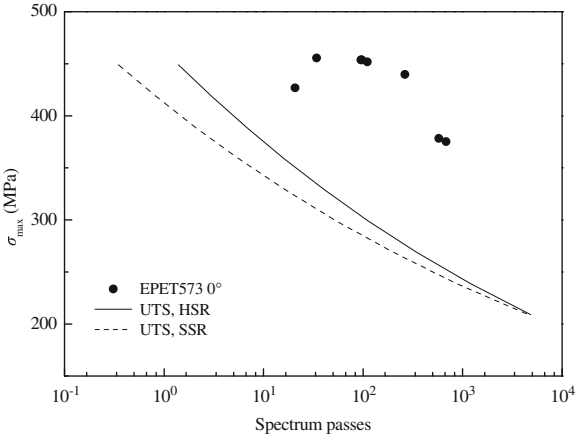

Fig. 7.21 Effect of ultimate tensile stress value on life prediction results. EPET573 spectrum applied on-axis (HSR: high strain rate, SSR: standard strain rate)

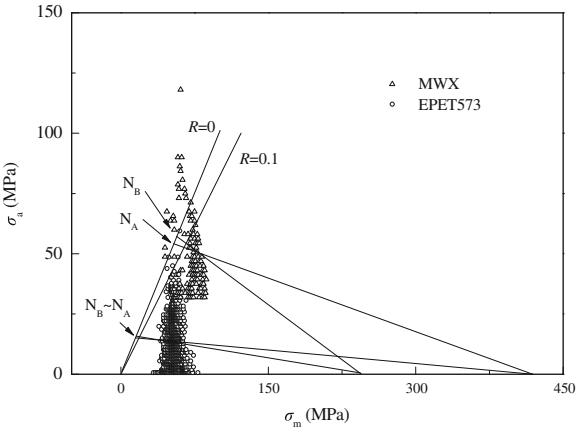

Fig. 7.22 Calculation of allowable number of cycles for selected bins of both spectra using different UTS values

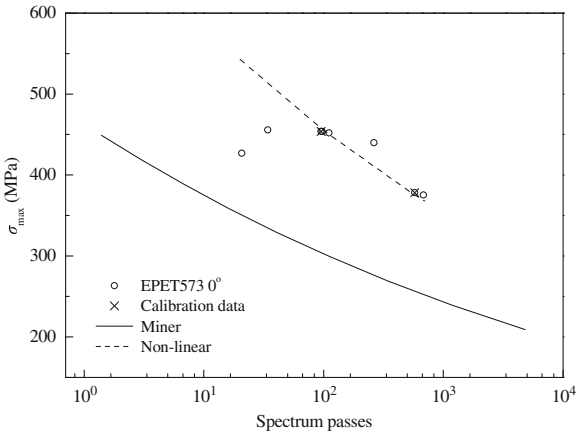

Fig. 7.23 Comparison of life prediction using Miner and non-linear rule. EPET573 spectrum applied on-axis. ($A = 2$, $B = 2$, $c = 1.001826$)

specimens tested under the EPET573 spectrum is examined, although in this case the influence of static strength value is proved less significant, see Fig. 7.21.

This can be explained by Fig. 7.22 where rainflowed data from both time series are projected on the (σ_m–σ_a)-plane. Open triangles correspond to blocks, containing numbers of cycles, part of the 12,831 cycles of the MWX spectrum, with the same range and mean value, while open cycles refer to CA blocks of the EPET573 spectrum.

As MWX contains cycles with higher amplitude and mean values than the EPET573 spectrum, and considering the form of the constant life diagrams used, it is obvious that a higher UTS value would produce less conservative predictions than a lower one. The allowable number of cycles for each block is determined by linear interpolation between known values on the CLD, for example, UTS and the S–N curve at $R = 0.1$, as shown in Fig. 7.22. The intersection of the S–N curve and the straight line passing through the UTS and each block defines the allowable number of cycles for the current block. Thus, as shown in Fig. 7.22, significantly different numbers of allowable cycles are calculated when rainflowed data from the MWX spectrum are analyzed. On the other hand, it is obvious that when counted cycles of lower range and mean values are examined, typical of those of the EPET573 spectrum, the difference between the calculated allowable number of cycles, using high or low UTS values, is not as great.

Life predictions can be drastically improved if a limited number of VA test data is used to determine the parameters of the non-linear fitting equation (Eq. 7.3). Then, keeping the same parameter values, the number of spectrum passes to failure for other specimens, i.e., different maximum stress levels, is accurately predicted. For example, in Fig. 7.23, model parameters are adjusted by using experimental data from EPET573 at 0°, denoted by the symbol ×, and predictions for the remaining test data points are considerably improved compared with the linear damage accumulation rule.

In Fig. 7.24, the same procedure was used to predict the life of specimens tested off-axis at 30° and 60°, under EPET573, with clearly satisfactory results.

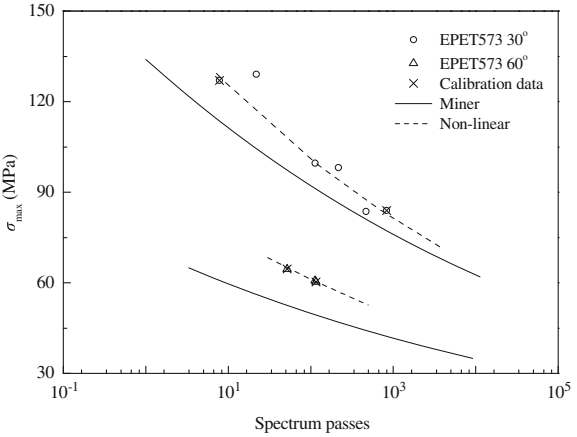

Fig. 7.24 Comparison of life prediction using Miner and non-linear rule. EPET573 spectrum applied on 30° ($A = 1.5$, $B = -1.5$, $c = 1.0529$) and 60° ($A = 1.5$, $B = -1.5$, $c = 1.0127$) off-axis specimens

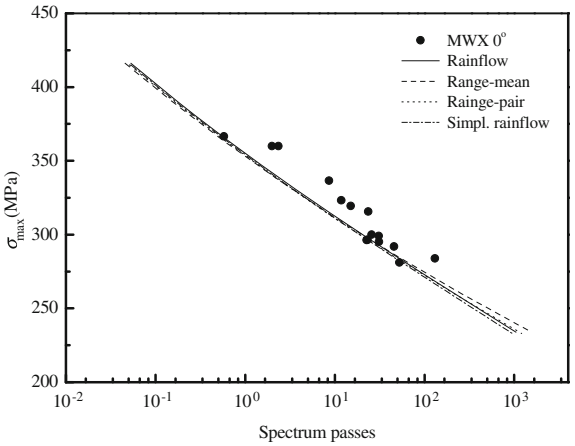

Fig. 7.25 Effect of different cycle-counting methods on life prediction results. MWX spectrum applied on-axis

7.3.3 Alternative Configurations

Although the presented results are based on a simple sequence of solvers selected for the solution of each step of the classic fatigue life prediction methodology, alternative configurations can also be selected for determination of the damage coefficient in order to investigate the effect of each solver on life prediction results.

7.3.3.1 Effect of Cycle-Counting Method

As shown in Fig. 7.25 for the MWX spectrum, predictions using the classic fatigue life methodology are corroborated by the experimental data, irrespective of the cycle-counting algorithm used. However, this is not the case for the EPET573

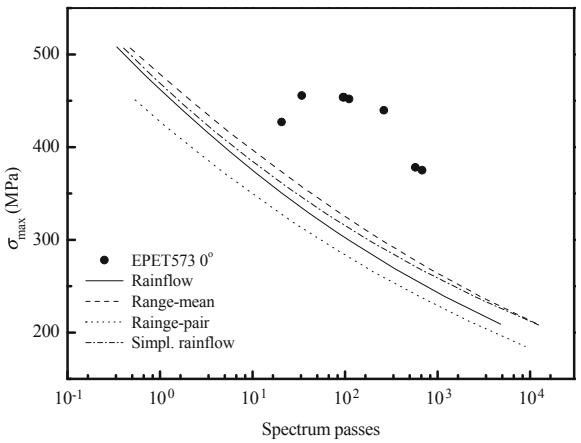

Fig. 7.26 Effect of different cycle-counting methods on life prediction results. EPET573 spectrum applied on-axis

spectrum, as shown in Fig. 7.26. As previously mentioned, see Fig. 7.16, the life prediction for this spectrum using the standard configuration was not accurate. Nevertheless, as presented in Fig. 7.26 use of the range-mean cycle-counting technique improves the predictions for the EPET573 spectrum compared to the results obtained from the application of the other (rainflow-related) techniques.

One reason for this could be the extreme and frequent load transitions in the EPET573 time series and the characteristic of rainflow counting-related methods to "produce" cycles that do not really exist, as they conjugate unrelated parts from throughout the time series. Thus, when the time series consists of extreme and frequent load transitions, such as EPET573, the phenomenon is intensified and differences in the numbers of cycles counted by rainflow-related and single range-mean methods are more evident. For the smoother MWX time series however, this is not the case, as a considerable number of cycles counted using rainflow-related methods are formed from adjacent load reversals.

It is demonstrated that all examined cycle-counting methods can be used as part of the entire life prediction methodology and provide more or less accurate results depending on the examined material and applied loading spectrum. It should nevertheless be noted that these comments must be validated by additional comparisons between predictions and other experimental data, considering different loading spectra and/or different material systems.

7.3.3.2 Effect of S–N Curve Formulation

The selection of the S–N curve formulation was also found to affect the life prediction results for the examined material and the applied variable amplitude spectra. As shown in Fig. 7.27, the two formulations based on the Log-Log equation (the linear log S vs. log N regression and the method proposed by Whitney) provide similar and quite accurate results. The semi-logarithmic (Lin-Log) equation

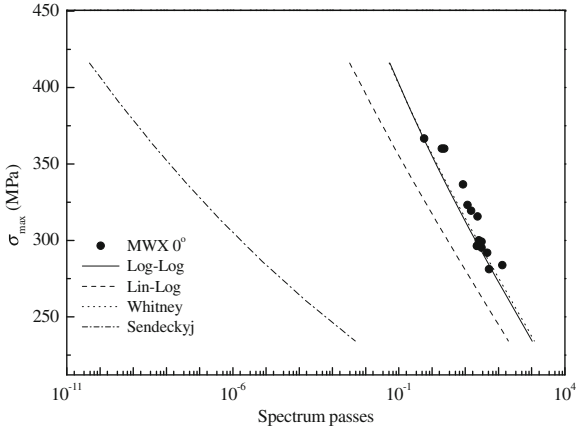

Fig. 7.27 Effect of different S–N formulations on life prediction results. MWX spectrum applied on-axis

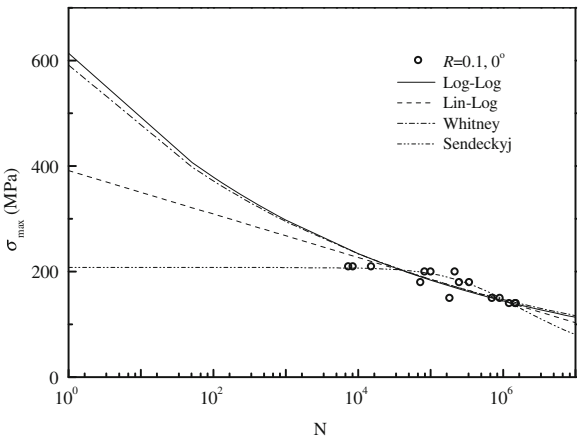

Fig. 7.28 Modeling of low-cycle fatigue regime by different S–N curve formulations

is less accurate as it becomes conservative, while the prediction from the Sendeckyj wear-out model is far less accurate when estimating failure at very early stages of loading.

In Fig. 7.28 the S–N curves derived by the different methods are presented for the *R*-ratio of 0.1, the closest available to the average stress ratio observed in the MWX variable amplitude spectrum. As shown in this figure, the S–N curves based on the Log-Log formulation overestimate the life in the low-cycle fatigue regime, estimating the tensile strength of the material at a value of around 600 MPa, roughly 1.5 times higher than the experimentally derived static strength obtained at a high loading rate (see Chap. 2). The S–N curve derived based on the semi-logarithmic equation models well the behavior in the low-cycle regime, but underestimates the behavior for high-cycle fatigue. The curve derived by the wear-out model without using the static data however is very conservative in the low-cycle fatigue regime. According to this S–N curve, even one cycle with a

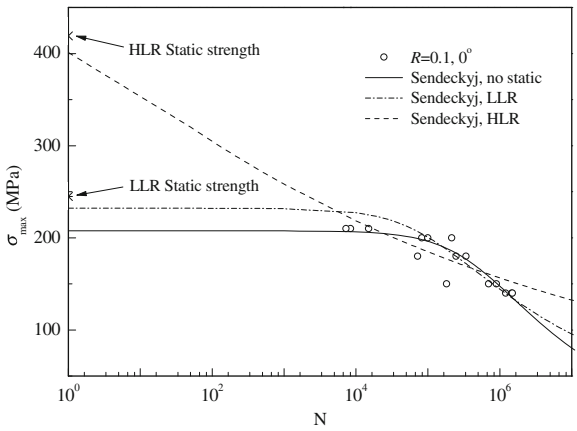

Fig. 7.29 S–N curves based on wear-out model, including and excluding static strength data

maximum stress of more than 200 MPa can produce failure of the examined on-axis specimens, something that is obviously not true.

As mentioned in Chap. 2—where the variable amplitude spectra were analytically presented—MWX has no cycles with a range lower than 30% of its maximum. Therefore, modeling of the low-cycle fatigue regime is critical for the life prediction of materials loaded under this spectrum. Although no fatigue data are available in the low-cycle fatigue regime for the examined material, use of the static strength data can improve the modeling of the constant amplitude fatigue behavior in the range between 1 and 100 cycles. An example is given in Fig. 7.29, which shows the S–N curves derived based on the Sendeckyj wear-out model including and excluding static strength data.

As shown in Fig. 7.29 using the static strength data considerably improve the constant amplitude fatigue life modeling of the on-axis loaded specimens in the low-cycle fatigue region. The resulting S–N curve, after using the static strength data derived under a loading rate similar to that of the fatigue experiments, designated HLR, is similar to the Lin-Log curve (shown in Fig. 7.28) for low cycles and becomes less conservative than the Lin-Log for longer fatigue lives. On the other hand, the S–N curve derived using the static strength data obtained from standard loading rate experiments is still low, although improved, compared to the S–N curved derived without the use of any static strength values. These differences are reflected in the life prediction results presented in Fig. 7.30 where, as shown, life prediction accuracy is very much improved when the HLR static strength data are also used. In this case, the predicted results are similar to those produced using the Log-Log S–N curve.

All in all, it has been shown in this section that the examined S–N curve formulations can, under certain conditions, be used in the framework of the classic fatigue life prediction methodology and provide relatively accurate results. The Log-Log formulation based on simple linear regression analysis and easily applied to any material fatigue dataset, even by hand calculations, was proved the most reliable and provided the most accurate results within the framework of the life

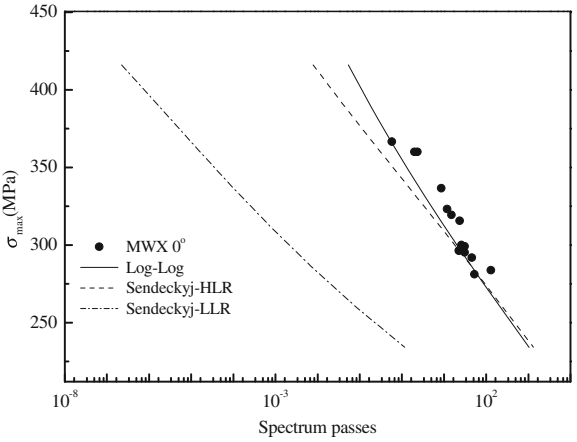

Fig. 7.30 Life prediction results using S–N curves derived by the wear-out model with and without static strength data. MWX spectrum applied on-axis

prediction methodology. However, when greater reliability is necessary, more complex models like Whitney's pooling scheme and Sendeckyj's wear-out model must be employed. In that case however, the results must be considered with caution since the derived curves can be misleading if the appropriate dataset is not analyzed, as was proved in the examined case for the wear-out model without the use of static strength data.

7.3.3.3 Effect of Constant Life Diagram Formulation

Modeling of the constant amplitude fatigue behavior of the examined material is very important within the framework of the fatigue life prediction methodology used here. One step in constant amplitude fatigue modeling is the derivation of the appropriate S–N curves, while the other is the construction of the constant life diagrams, based on which new S–N curves for any desired R-ratio must be predicted. All the models for the derivation of a constant life diagram described in Chap. 4 have been applied and selected results are presented in Fig. 7.31 for discussion. For application of the linear model, the S–N curve corresponding to reversed fatigue ($R = -1$) was used, while three S–N curves (under $R = 10, -1$ and 0.1) were used for derivation of the rest of the diagrams. Comparison of the results shows that the piecewise linear and Boerstra models are the most appropriate for the examined material under the given loading conditions and these results are presented in Fig. 7.31. The other diagrams, Harris, Harris-power, Kawai and piecewise non-linear (see Chap. 4 for details), yielded similar life predictions—those of piecewise non-linear are plotted in Fig. 7.31—while the linear diagram yielded very conservative predictions.

The explanation concerning the results presented in Fig. 7.31 is given in Fig. 7.32 where different constant life diagrams are shown for selected numbers of cycles together with the experimentally derived data from on-axis specimens

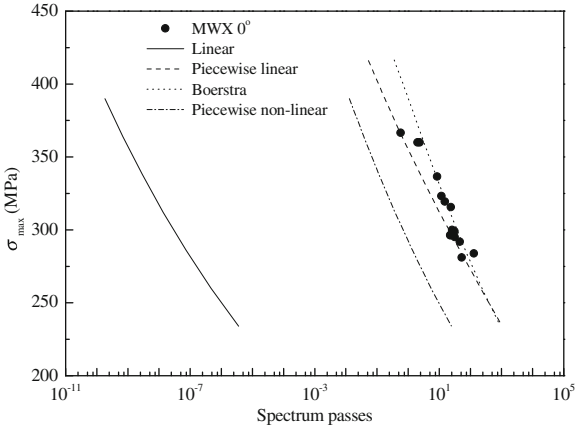

Fig. 7.31 Life prediction results using different CLD models. Configuration: Rainflow-counting, Log-Log S–N curves, CLD, Miner. MWX spectrum applied on-axis

loaded under $R = 0.5$. The numbers of cycles correspond to the mean value of the estimated fatigue life per examined stress level and the relationship of the corresponding curves with the data points defines the accuracy of each presented model. As shown in this figure, the linear diagram predicts a very conservative S–N curve for the $R = 0.5$ loading case, while the piecewise non-linear yields a conservative curve but still within the experimental data range. The piecewise linear and Boerstra diagrams on the other hand are non-conservative for low numbers of cycles up to around 5×10^3 and become very accurate for numbers above 10^5. This performance is very obvious in the case of the Boerstra diagram results shown in Fig. 7.31. Use of this diagram overestimates the fatigue life of the examined material under the given loading conditions for high stress levels—low-cycle fatigue—but it becomes very accurate for lower applied loads, corresponding to higher numbers of cycles.

7.3.3.4 Effect of the Multiaxial Fatigue Failure Criterion

All multiaxial fatigue theories, except those presented by Kawai et al. and Shokrieh and Taheri (see Chap. 6 for details), were used for the prediction of the fatigue life of the examined material system under the multiaxial stress states developed as a result of the application of MWX and EPET573 variable amplitude spectra. The results, presented in Figs. 7.33, 7.34, show that all employed multiaxial fatigue failure criteria are able to produce relatively accurate life predictions, independent of the applied variable amplitude spectrum.

For application of the FWE criterion, reference curves from specimens tested under the same R-ratio as the examined one were used, although the stress ratio effect is taken into account by the criterion formulation. However, it has been proved elsewhere [26] that the selection of a reference curve from another dataset (from tests under a different stress ratio than that of the curve to be predicted) can produce highly inaccurate results. For the results shown in Figs. 7.33, 7.34 the

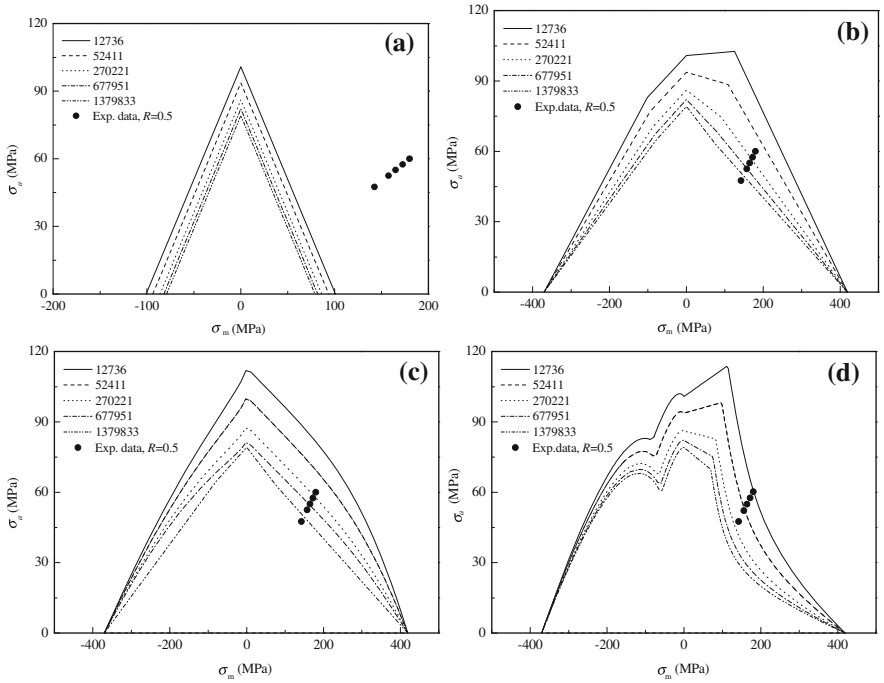

Fig. 7.32 Modeling of constant amplitude fatigue life for $R = 0.5$, on-axis specimens. **a** Linear. **b** Piecewise linear. **c** Boerstra. **d** Piecewise non-linear

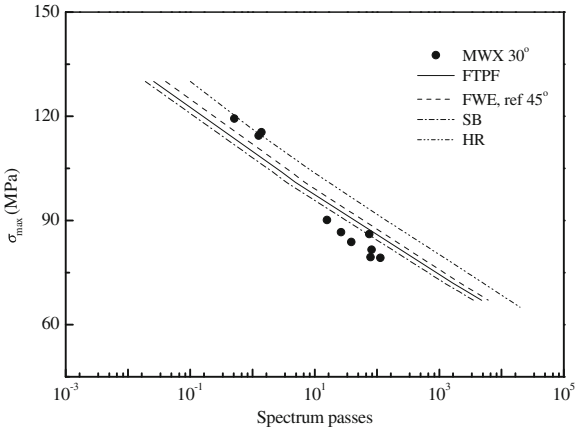

Fig. 7.33 Lifetime estimation according to different multiaxial fatigue failure criteria. MWX spectrum applied on 30° off-axis specimens

S–N curve at 45° was used as the reference for the FWE criterion, although according to the theory there is no restriction as to which curve must be used. However, the ability of the examined fatigue theories to predict fatigue life under variable amplitude complex stress states is strongly affected by their accuracy when off-axis S–N curves are estimated. Therefore, as described in Chap. 6, the

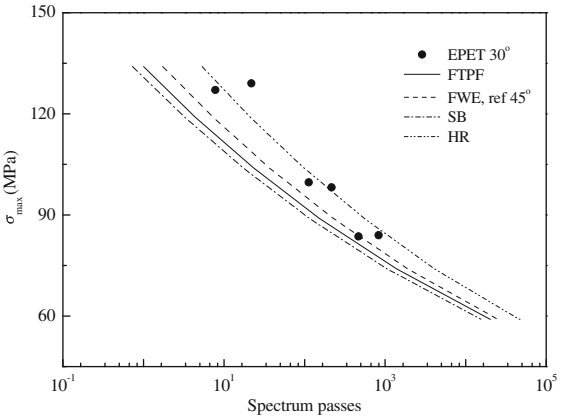

Fig. 7.34 Lifetime estimation according to different multiaxial fatigue failure criteria. MWX spectrum applied on 30° off-axis specimens

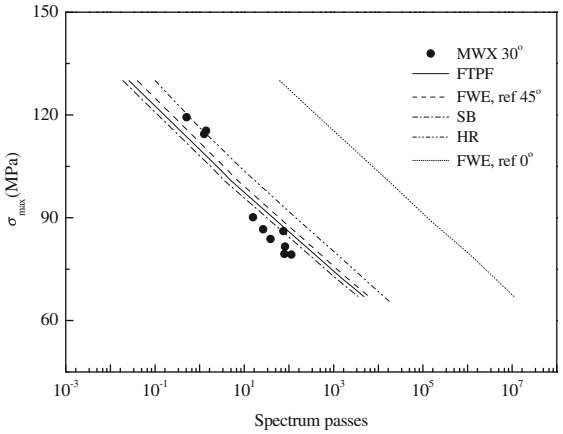

Fig. 7.35 Lifetime estimation according to different multiaxial fatigue failure criteria. FWE ref 45° and FWE ref 0° comparison. MWX spectrum applied on 30° off-axis specimens

polynomial-based fatigue failure criteria, such as FTPF, HR and SB, are reliable in variable amplitude fatigue modeling since they also accurately predicted the off-axis fatigue behavior. In contrast the FWE criterion, together with other fatigue theories based on a master fatigue curve and relevant static strength data, yield accurate (see Figs. 7.33, 7.34) or highly inaccurate results (see Fig. 7.35) depending on the selected reference curve, and once again proved very sensitive to the selection of the reference fatigue curve.

7.4 Conclusions

The accuracy of the prediction of the lifetime of composite materials under variable amplitude loading is based on the accuracy of a series of processes before reaching the final goal. The theoretical background along with a thorough

experimental verification of a life prediction methodology for multidirectional composite laminates under irregular load sequences has been presented in this chapter. Although the procedure could be applicable for 3D stress states, the actual implementation of both the theoretical formulation and material database is limited to plane stress conditions. Furthermore, loading spectra are assumed to produce a plane stress state in which components of the stress tensor are proportional time series. This requirement is imposed by the cycle-counting method implemented in the computational procedure.

Material property evaluation follows a direct characterization approach; the laminated plate is tested in its symmetry directions and respective fatigue strength parameters are derived. The proposed procedure is therefore suitable for the life prediction of a structural component designed for ultimate (static) or stability critical loads. If fatigue design optimization is required, a "ply-to-laminate" prediction methodology and associated ply characterization techniques should be adopted instead.

The algorithm consists mainly of five routines: cycle counting for the variable amplitude spectrum, derivation of the appropriate S–N curves for the modeling of the constant amplitude fatigue behavior of the materials, formulation of constant life diagrams to take into account the mean stress effect on the fatigue life of the examined material, derivation of allowable numbers of cycles using multiaxial fatigue failure criteria and finally, damage accumulation. Although specific choices for each one of the above routines were made, the method could in principle be implemented for any possible configuration, as the only success criterion is good prediction of the experimental results.

Nevertheless, for the cycle counting, the rainflow-counting algorithm was selected, the Log-Log S–N curve type was used together with the piecewise linear constant life diagram for the modeling of the constant amplitude fatigue data, whereas fatigue strength under multidimensional stress states was assessed using the FTPF multiaxial fatigue failure criterion because of its efficiency in satisfactorily predicting the fatigue behavior of many different composite material systems under various loading conditions. Finally, the Miner linear damage rule was adopted for the damage summation because of its simplicity and because it is the only widely accepted predictive scheme that does not require any fitting procedures on the experimental results. Furthermore, it yields successful results for GRP laminated composites in general. If necessary, non-linear regression models could be evaluated to improve the accuracy of theoretical calculations.

To demonstrate the procedure, experimental results from an extensive experimental program consisting of static and fatigue tests on specimens cut on- and off-axis from a multidirectional GRP laminate were used. Variable amplitude and constant amplitude fatigue experiments under various R-ratios were performed. Plane stress states were simulated by loading the specimens off-axis, thus developing proportional time series of stress tensor components, though of different maximum, minimum and mean values.

Implementation of the method to predict the number of spectrum passes applied to test specimens loaded on- and off-axis at 30^{o} and 60^{o}, using two different

irregular load histories, yielded satisfactory results and proved the suitability of the procedure for the GRP laminate investigated. However, prediction accuracy was found to be dependent on several parameters such as the load spectrum, baseline data, constant life diagram, fatigue failure criterion and damage accumulation rule and this point merits further examination.

Different life predictions were also produced when static strengths, UTS and UCS, determined according to relevant standards, were used instead of those at a similar strain rate to that of the fatigue tests. Generally, it was found that if static strength data should be combined with available fatigue data in order to derive S–N curves and constant life diagrams, the static and fatigue data must be derived under the same conditions–in this case loading rates.

The use of a non-linear equation to fit the fatigue behavior of the GRP laminate investigated under variable amplitude loading was proved feasible. The resulting predictions were accurate, improving in all the examined cases those derived using the Miner linear damage rule. The major drawback in using such a non-linear life prediction scheme is the requirement of a small number of experimental data under each examined spectrum. It is therefore not practical for applications involving a large number of different fatigue load cases.

A parametric study was performed in this chapter to examine the effect of the existing solvers for the each step of the classic life prediction methodology on the theoretical results. The accuracy of some of the examined configurations in predicting the fatigue life of the examined composite material systems under both applied variable amplitude spectra is acceptable. The application of the methodology proved to be easy and straightforward without the need for any complicated numerical solutions. However, experience showed that some of the solvers can be accurate for one material and examined loading case but highly inaccurate for another, as was proved for example in this chapter with the wear-out model and constant amplitude fatigue life modeling by including and excluding static strength data.

A commonly accepted complete fatigue theory does not yet exist, although some of the sub-problems have already been successfully addressed. Software frameworks like *CCfatigue* can assist the development process of a unified fatigue life prediction methodology by comparing the life prediction results produced by different solver configurations and validating theoretical life prediction results against variable amplitude loading experimental data from different material systems.

References

1. G.P. Sendeckyj, in *Life Prediction for Resin-Matrix Composite Materials in Fatigue of Composite Materials*, vol. 4, ed. by K.L. Reifsnider, Composite Materials Series 4 (Elsevier, Amsterdam, 1991)
2. T. Adam, N. Gathercole, H. Reiter, B. Harris, Life prediction for fatigue of T800/5245 carbon-fibre composites: II Variable-amplitude loading. Fatigue **16**(8), 533–547 (1994)
3. I.P. Bond, Fatigue life prediction for GRP subjected to variable amplitude loading. Compos. Part A Appl. Sci. **30**(8), 961–970 (1999)

4. W. Hwang, K.S. Han, Cumulative damage models and multi-stress fatigue prediction. J. Compos. Mater. **20**(2), 125–153 (1986)
5. M.J. Owen, R.J. Howe, The accumulation of damage in a glass-reinforced plastic under tensile and fatigue loading. J. Phys. D Appl. Phys. **5**(9), 1637–1649 (1972)
6. J.R. Schaff, B.D. Davidson, Life prediction methodology for composite structures. Part II spectrum fatigue. J. Compos. Mater. **31**(2), 158–181 (1997)
7. L.J. Broutman, S. Sahu, A new theory to predict cumulative fatigue damage in fiberglass reinforced plastics. in *Proceedings of the 2nd Conference on Composite Materials: Testing and Design, ASTM STP 497*, (1972) pp. 170–188
8. W.X. Yao, N. Himmel, A new cumulative fatigue damage model for fibre-reinforced plastics. Compos. Sci. Technol. **60**(1), 59–64 (2000)
9. W. Hwang, K.S. Han, Fatigue of composites-fatigue modulus concept and life prediction. J. Compos. Mater. **20**(2), 154–165 (1986)
10. L.J. Lee, K.E. Fu, J.N. Yang, Prediction of fatigue damage and life for composite laminates under service loading spectra. Compos. Sci. Technol. **56**(6), 635–648 (1996)
11. W.F. Wu, L.J. Lee, S.T. Choi, A study of fatigue damage and fatigue life of composite laminates. J. Compos. Mater. **30**(1), 123–137 (1996)
12. R.P.L. Nijssen, OptiDAT–fatigue of wind turbine materials database (2006) http://www.kc-wmc.nl/optimat_blades/index.htm
13. J.F. Mandell, D.D. Samborsky, DOE/MSU Composite Material Fatigue Database. Sandia National Laboratories, SAND97-3002, (online via www.sandia.gov/wind, v. 18, 21st March (2008) Updated)
14. C.W. Kensche, in *GFRP Fatigue Data for Certification in European Wind Energy Conference Proceedings*, vol. I, (Thessaloniki, Greece, 1994) pp. 738–742
15. P.W. Bach, P.A. Joosse, D.R.V. van Delft, Fatigue lifetime of glass.polyester laminates for wind turbines. in *The European Wind Energy Conference Proceedings*, vol. I (Thessaloniki, Greece 1994), pp. 94–99
16. S.I. Andersen, P.W. Bach, W.J.A. Bonee, C.W. Kensche, H. Lilholt, A. Lystrup, W. Sys, in *Fatigue of Materials and Components for Wind Turbine Rotor Blades*. ed. by C.W. Kensche, Directorate-General XII, Science, Research and Development, EUR 16684 EN (1996)
17. T.P. Philippidis, A.P. Vassilopoulos, Life prediction methodology for GFRP laminates under spectrum loading. Compos. Part A Appl. S. **35**(6), 657–666 (2004)
18. Y. Zhang, A.P. Vassilopoulos, T. Keller, Environmental effects on fatigue behavior of adhesively–bonded pultruded structural joints. Compos. Sci. Technol. **69**(7–8), 1022–1028 (2009)
19. T.P. Philippidis, E.N. Eliopoulos, A progressive damage mechanics algorithm for life prediction of composite materials under cyclic complex stress. in *Fatigue Life Prediction of Composites and Composite Structures*, ed. by A.P. Vassilopoulos (Woodhead publishing Ltd, Cambridge 2010)
20. T.P. Philippidis, A.P. Vassilopoulos, Complex stress state effect on fatigue life of GFRP laminates. Part I, Experimental. Int. J. Fatigue **24**(8), 813–823 (2002)
21. T.P. Philippidis, A.P. Vassilopoulos, Complex stress state effect on fatigue life of GRP laminates. Part II, Theoretical formulation. Int. J. Fatigue **24**(8), 825–830 (2002)
22. T.P. Philippidis, A.P. Vassilopoulos, Fatigue strength of composites under variable plane stress. in *Fatigue in Composite*, Chap. 18. ed. by B. Harris (Woodhead Publishing and CRC Press, Cambridge 2003), pp. 504–525
23. T.W. Coats, C.E. Harris, Experimental verification of a progressive damage model for IM7/5260 laminates subjected to tension–tension fatigue. J. Compos. Mater. **29**(3), 280–305 (1995)
24. M.M. Shokrieh, L.B. Lessard, Progressive fatigue damage modelling of composite materials, Part I: Modeling. J. Compos. Mater. **34**(13), 1056–1080 (2000)
25. http://www.fireholetech.com/products/helius-fatigue.aspx
26. A.P. Vassilopoulos, R. Sarfaraz, B.D. Manshadi, T. Keller, A computational tool for the life prediction of GFRP laminates under irregular complex stress states: Influence of the fatigue failure criterion. Comp. Mater. Sci. **49**(3), 483–491 (2010)

27. ASTM E1049–85 (2005) Standard practices for cycle counting in fatigue analysis
28. R.P.L. Nijssen, Fatigue life prediction and strength degradation of wind turbine rotor blade composites. PhD Thesis, TU Delft; 2006, ISBN–13:978–90–9021221–0
29. T. Endo, K. Mitsunaga, H. Nakagawa, Fatigue of metals subjected to varying stress – Prediction of fatigue lives, preliminary proceedings of the Chigoku–Shikoku District Meeting, Japan Society of Mechanical Engineers, November 1967 pp. 41–44
30. M. Matsuishi, T. Endo, Fatigue of metals subjected to varying stress – Fatigue lives under random loading, preliminary proceedings of the Kyushu District Meeting, Japan Society of Mechanical Engineers (1968) pp. 37–40
31. J.B. de Jonge, The analysis of load–time histories by means of counting methods. in *Helicopter fatigue design guide*, ed. by F. Liard AGARD–AG–292, (November 1983)
32. S.D. Dowling, D.F. Socie, Simple rainflow counting algorithms. Int. J. Fatigue **4**(1), 31–40 (1982)
33. A. Fatemi, L. Yang, Cumulative fatigue damage and life prediction theories: A survey of the state of the art for homogeneous materials. Int. J. Fatigue **20**(1), 9–34 (1998)
34. I.P. Bond, I.R. Farrow, Fatigue life prediction under complex loading for XAS/914 CFRP incorporating a mechanical fastener. Int. J. Fatigue **22**(8), 633–644 (2000)